

Calculation of the time resolution of the J-PET tomograph using kernel density estimation

L Raczynski¹, W Wiślicki¹, W Krzemień², P Kowalski¹,
D Alfs³, T Bednarski³, P Białas³, C Curceanu⁴, E Czerwiński³,
K Dulski³, A Gajos³, B Głowacz³, M Gorgol⁵, B Hiesmayr⁶,
B Jasińska⁵, D Kamińska³, G Korcyl³, T Kozik³, N Krawczyk³,
E Kubicz³, M Mohammed³, M Pawlik-Niedźwiecka³,
S Niedźwiecki³, M Pałka³, Z Rudy³, O Rundel³, N G Sharma³,
M Silarski³, J Smyrski³, A Strzelecki³, A Wieczorek³,
B Zgardzińska⁵, M Zieliński³ and P Moskal³

¹ Department of Complex Systems, National Centre for Nuclear Research, 05-400 Otwock-Świerk, Poland

² High Energy Physics Division, National Centre for Nuclear Research, 05-400 Otwock-Świerk, Poland

³ Faculty of Physics, Astronomy and Applied Computer Science, Jagiellonian University, 30-348 Cracow, Poland

⁴ INFN, Laboratori Nazionali di Frascati, 00044 Frascati, Italy

⁵ Institute of Physics, Maria Curie-Skłodowska University, 20-031 Lublin, Poland

⁶ Faculty of Physics, University of Vienna, 1090 Vienna, Austria

E-mail: lech.raczynski@ncbj.gov.pl

Received 19 December 2016, revised 7 April 2017

Accepted for publication 28 April 2017

Published 26 May 2017



Abstract

In this paper we estimate the time resolution of the J-PET scanner built from plastic scintillators. We incorporate the method of signal processing using the Tikhonov regularization framework and the kernel density estimation method. We obtain simple, closed-form analytical formulae for time resolution. The proposed method is validated using signals registered by means of the single detection unit of the J-PET tomograph built from a 30 cm long plastic scintillator strip. It is shown that the experimental and theoretical results obtained for the J-PET scanner equipped with vacuum tube photomultipliers are consistent.

Keywords: positron emission tomography, time resolution, kernel density estimation

(Some figures may appear in colour only in the online journal)

1. Introduction

The Jagiellonian PET (J-PET) Collaboration has constructed a PET scanner using plastic strips to form the barrel (Moskal *et al* 2011, 2014a). An example of the arrangement of the scintillator strips in the J-PET tomograph is shown in figure 1. The proposed setup permits the use more than one detection layer, thus increasing the efficiency of γ photon registration (Moskal *et al* 2016). A single detection module consists of a long scintillator strip and a pair of photomultipliers attached to opposite ends of the strip. Measurement with such a detector results in timestamps from both sides of each scintillator, allowing the timing, position and energy information for each γ photon interaction to be extracted. The time and position of the γ photon interaction in the scintillator strip is calculated based on times at the left ($t_{(L)}$) and right ($t_{(R)}$) side of the strip. In the first approximation, the time of interaction may be estimated as an arithmetic mean of $t_{(L)}$ and $t_{(R)}$ and the position of interaction along the strip may be calculated as $(t_{(L)} - t_{(R)})v/2$, where v denotes the speed of light signals in the scintillator strip. The energy deposited in the scintillator strip may be expressed in terms of the number of photoelectrons registered by the photomultipliers and is proportional to the arithmetic mean of a number of photoelectrons registered at the left and right sides of the scintillator; the energy calibration factor was evaluated in Moskal *et al* (2014b). Registration of a single event of positron emission, used for image reconstruction, is based on the detection of both γ photons in two modules in a narrow time window. Therefore, a single image-building event includes information about four arrival times of light signals at the left and right ends of the two modules that register in coincidence. The J-PET detector offers time of flight (TOF) resolution competitive with existing solutions (Humm *et al* 2003, Townsend 2004, Karp *et al* 2008, Conti 2009, 2011, Słomka *et al* 2016), due to the fast plastic scintillators and dedicated electronics allowing for sampling in the voltage domain of signals with durations of a few nanoseconds (Palka *et al* 2014).

Recently, a time resolution, defined hereafter as the standard deviation, of about 80 ps has been achieved for the registration of γ photons in 30 cm long scintillator strips read out at both ends by the vacuum tube photomultipliers (Moskal *et al* 2014b, Raczynski *et al* 2014). Such resolution results in a coincidence resolving time (CRT) of about 275 ps, as shown in Moskal *et al* (2016). Further improvement in the time resolution requires developments in techniques of signal processing and effective parametrizations of detector features. Our estimate of the time resolution is based on statistical properties of the signals in plastic scintillators. The distribution of the time of photon emission followed by its interaction in plastic scintillators was described in Moszynski and Bengtson (1977) and Moszynski and Bengtson (1979). Following the time order statistics analysis described, for example, in Seifert *et al* (2012), DeGroot (1986) and Spanoudaki and Levin (2011), a statistical framework allowing for the analysis of photon propagation in the scintillator strips was proposed in Moskal *et al* (2016).

In this paper we propose a novel approach to calculate the time resolution of the PET scanner based on ideas from Tikhonov regularization (Tikhonov 1963, Tikhonov and Arsenin 1977) and kernel density estimation (Rosenblat 1956, Parzen 1962) methods. We investigate the quality of time resolution estimates based on the scheme with a single scintillator strip detector introduced in Moskal *et al* (2014b) and Raczynski *et al* (2014). The most important aspect of evaluating time resolution involves the statistical description of noise. The noise in the measured signal comprises two components: statistical fluctuations of the number of photoelectrons registered by the photosensor, and the effect of the limited number of samples of the signal in the voltage domain. In Raczynski *et al* (2015a), a formula for calculating the signal recovery error was introduced and proved. In this paper we determine the dependence of the signal estimation error on the number and shape of registered photoelectron signals.



Figure 1. Schematic of an example of a three-layer J-PET detector. Each scintillator strip is aligned axially and read out at two ends by photomultipliers.

Theoretical results are compared with the experimental resolutions achievable using traditional readout with vacuum tube photomultipliers. The method is verified by using in the calculations the same conditions as in the experiment, as described in Moskal *et al* (2014b) and Raczynski *et al* (2014).

The J-PET tomograph can be equipped with various types of photomultiplier: vacuum tube photomultipliers (standard in the J-PET prototype), silicon photomultipliers or microchannel plate photomultipliers. In case of vacuum tube or silicon photomultipliers, registration of the whole signal is not possible, and therefore sampling in the voltage domain using a predefined number of voltage levels is needed. The output signal is then recovered using ideas from Tikhonov regularization (Tikhonov 1963, Tikhonov and Arsenin 1977) and compressive sensing (Candes *et al* 2006, Donoho 2006) methods. The microchannel plate photomultipliers are the most promising for application in the J-PET instrument due to the possibility of direct registration of the timestamp of each single photon. In the experimental study we will derive time resolutions of various configurations of the J-PET detector using different types of photomultiplier.

2. Materials and methods

In this work we assume that the γ photon interacts in the scintillator strip at time Θ and in position x . We consider resolution for these reconstructions.

The time of photon registration at the photomultiplier, referred to as t_r , is considered as a random variable equal to the sum of three contributing values:

$$t_r = t_e + t_p + t_d, \quad (1)$$

where t_e is the photon emission time, t_p is the propagation time of the photon along the scintillator strip and t_d is the photomultiplier transit time. Assuming that the times t_e, t_p, t_d , given in equation (1), are independent random variables with probability density functions (pdfs) denoted with $f_{t_e}, f_{t_p}, f_{t_d}$, respectively, the distribution function of t_r is given as the convolution

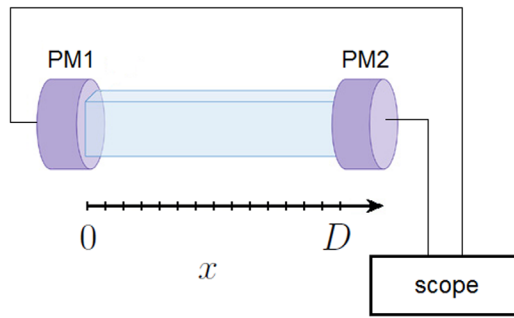


Figure 2. Measurement provided with a single scintillator strip. The variable x describes the position of the emission point along the strip.

$$f_r(t) = (f_{t_e} * f_{t_p} * f_{t_d})(t), \quad t > 0.$$

For the ternary plastic scintillators used in the J-PET detector (Saint Gobain Crystals 2017, Eljen Technology 2017), the distribution of t_e is well approximated by the following formula (Moszynski and Bengtson 1977, Moszynski and Bengtson 1979):

$$f_e(t) = \kappa_e \int_{\Theta}^t \left(e^{-\frac{t-\tau}{\tau_d}} - e^{-\frac{t-\tau}{\tau_r}} \right) e^{-\frac{(\tau-\Theta-2.5\sigma_e)^2}{2\sigma_e^2}} d\tau, \quad (2)$$

where $\tau_d = 1.5$ ns, $\tau_r = 0.005$ ns and $\sigma_e = 0.2$ ns, and κ_e stands for the normalization constant. The values of the parameters τ_d, τ_r, σ_e were adjusted in order to describe the properties of the light pulses from the BC-420 scintillator (Moskal *et al* 2016, Saint Gobain Crystals 2017). From the definition in equation (2):

$$t_e \geq \Theta. \quad (3)$$

The initial direction of flight of the photon in the scintillator is uniformly distributed. The photon on its way along the scintillator strip, from the emission point to the photomultiplier, may undergo many internal reflections, the number of which depends on the geometry of the scintillator and the photon emission angle. However, the space reflection symmetries of the cuboidal shapes considered in this article enable a significant simplification of the photon transport algorithm without following photon propagation in a typical manner. The statistical modeling of this phenomenon was presented in detail in Moskal *et al* (2016) and the analytical function describing the distribution function f_p may be expressed by the following formula:

$$f_p(t) = \frac{\kappa_p x}{t^2} e^{-\mu_{\text{eff}} vt}, \quad (4)$$

where v is the speed of light in the scintillator strip, μ_{eff} is the effective absorption coefficient for the scintillator material and κ_p the normalization constant. The longitudinal position of the emission point is $0 \leq x \leq D$ (see figure 2). The pdf function $f_p(t)$ in equation (4) is nonzero only for

$$t_p \geq \frac{x}{v}, \quad (5)$$

where $t_p = \frac{x}{v}$ corresponds to the photon flying along the strip.

Finally, the time of registration t_{rnr} is smeared using a Gaussian distribution centered on the mean transition time T_d and variance σ_d^2 estimated empirically:

$$f_d(t) = \frac{1}{\sqrt{2\pi}\sigma_d} \exp\left(-\frac{(t - T_d)^2}{\sigma_d^2}\right). \tag{6}$$

In this work, we assume that the signal registered at the photomultiplier output has the same functional dependence on the time as the f_t function. We assume that the signal $y \in \mathbb{R}^N$ is discretized by the oscilloscope. It is sampled at constant time intervals denoted with T_s . From the condition equations (3) and (5) it follows that the registration time t_r fulfills the inequality

$$t_r \geq \Theta + \frac{x}{v}.$$

It was assumed that the transition time $t_d \geq 0$. Therefore, the n th time sample is given by

$$t^{(n)} = nT_s + \Theta + \frac{x}{v} \quad n = 1, 2, \dots, N, \tag{7}$$

and the n th sample of the signal y is given as

$$y(n) = \beta(E, x)f_n, \quad \text{where } f_n = f_t(t^{(n)}) \quad n = 1, 2, \dots, N, \tag{8}$$

where $\beta(E, x)$ is a coefficient providing the scaling of the pdf function f_t in order to obtain the voltage signal

$$\beta(E, x) = \beta_E \beta_x.$$

The value of $\beta(E, x)$ depends on the energy deposited in the plastic scintillator during the γ photon interaction (β_E factor) and on the position of the γ photon interaction along the strip (β_x factor). The higher the value of the deposited energy, the higher the value of the β_E parameter and the higher the signal amplitude. The β_x term is necessary to describe absorption of photons propagating through the scintillator strip, since f_t only provides information about the shape of the signal (see equation (4)). Hence, the closer to the left end of the scintillator, the smaller x (see figure 2) and the larger β_x . Contributions of β_E to β are the same for both ends of the strip but β_x are different. Hereon, in order to simplify the notation of the parameter $\beta(E, x)$, we use only the symbol β .

2.1. Reconstruction of the interaction time and position

We denote the true values of the time and position of γ photon interaction by Θ^0 and x^0 , respectively, and the corresponding reconstructed values are denoted as $\hat{\Theta}, \hat{x}$. We add a random noise term $v_{(L,R)}$ to the signal $y_{(L,R)}$ at the left (L) and right (R) end of the strip. Hence a registered signals $\hat{y}_{(L)}$ and $\hat{y}_{(R)}$ may be expressed as

$$\hat{y}_{(L)}(\Theta^0, x^0) = y_{(L)}(\Theta^0, x^0) + v_{(L)}. \tag{9}$$

$$\hat{y}_{(R)}(\Theta^0, x^0) = y_{(R)}(\Theta^0, x^0) + v_{(R)}. \tag{10}$$

We assume that the noise $v_{(L)}$ and $v_{(R)}$ are uncorrelated and obey the same multivariate normal distribution:

$$v_{(L)}, v_{(R)} \sim \mathcal{N}(0, S), \tag{11}$$

where S is the covariance matrix of $\hat{y}_{(L)}$ and $\hat{y}_{(R)}$, and we introduce the notation

$$\Delta\Theta = \Theta^0 - \Theta,$$

$$\Delta x = x^0 - x.$$

According to the definitions of the theoretical (y) and registered (\hat{y}) signals, the reconstruction of $\hat{\Theta}, \hat{x}$ may be pursued by minimization of the function:

$$W(\Delta\Theta, \Delta x) = (y_{(L)} - \hat{y}_{(L)})(y_{(L)} - \hat{y}_{(L)})^T + (y_{(R)} - \hat{y}_{(R)})(y_{(R)} - \hat{y}_{(R)})^T. \quad (12)$$

The solutions $\hat{\Theta}, \hat{x}$ are found as:

$$(\Delta\hat{\Theta}, \Delta\hat{x}) = \arg \min W(\Delta\Theta, \Delta x) \quad (13)$$

where the hat denotes the estimators.

From equations (9)–(10) and (12) it is seen that the error function W is a positive-valued random variable. In order to determine $\Delta\hat{\Theta}$ we assume that the error of the time of interaction has a normal distribution:

$$\Delta\hat{\Theta} \sim \mathcal{N}(0, \sigma_{\Theta}^2), \quad (14)$$

where σ_{Θ} is the search time resolution of the J-PET instrument.

2.2. Determination of time resolution

In order to calculate the time resolution, W has to be examined near the minimum, $(0, 0)$. According to equation (12), the random variable $W(0, 0)$ may be expressed as

$$\begin{aligned} W(0, 0) &= v_{(L)} v_{(L)}^T + v_{(R)} v_{(R)}^T, \\ &= \sum_{n=1}^N v_{(L)}^2(n) + v_{(R)}^2(n). \end{aligned} \quad (15)$$

The variance of W in the minimum will be denoted hereafter as $\text{Var}[W_{\min}]$. Using equation (11), and assuming the diagonality of matrix S , yields

$$\text{Var}[W_{\min}] = 2 \sum_{n=1}^N 2S^2(n, n). \quad (16)$$

On the other hand, we may analyse the shape of the function W in the two-dimensional space of time ($\Delta\hat{\Theta}$) and position ($\Delta\hat{x}$) errors. For the purpose of this work, we will consider only the ($\Delta\hat{\Theta}$) error, and therefore analyse W in one dimension ($\Delta\hat{x} = 0$). Taylor series expansion of W around $(0, 0)$ is given as:

$$\begin{aligned} W(\Delta\hat{\Theta}, 0) &\approx W(0, 0) + \frac{\partial W(0, 0)}{\partial \Delta\hat{\Theta}} \Delta\hat{\Theta} + \frac{1}{2} \frac{\partial^2 W(0, 0)}{\partial \Delta\hat{\Theta}^2} \Delta\hat{\Theta}^2 \\ &\approx \alpha_0 + \alpha_1 \Delta\hat{\Theta} + \alpha_2 \Delta\hat{\Theta}^2. \end{aligned} \quad (17)$$

It is evident that the first two coefficients (α_0, α_1) are equal to zero and the quadratic approximation simplifies to

$$W(\Delta\hat{\Theta}, 0) \approx \alpha_2 \Delta\hat{\Theta}^2. \quad (18)$$

Under the assumption of normality of the $\Delta\hat{\Theta}$ distribution (see equation (14)) the random variable $W(\Delta\hat{\Theta}, 0)$ given in equation (18) has a χ^2 distribution with variance

$$\text{Var}[W_{\min}] \approx 2\alpha_2^2 \sigma_{\Theta}^4. \quad (19)$$

The comparison of two formulae describing $\text{Var}[W_{\min}]$ in equations (19) and (16) enables us to determine the time resolution, defined as the standard deviation σ_{Θ} :

$$\sigma_{\Theta} = \sqrt[4]{\frac{2 \sum_{n=1}^N S^2(n, n)}{\alpha_2^2}}. \quad (20)$$

2.3. Determination of the coincidence resolving time

In order to facilitate the direct comparison with results published in the field of TOF-PET we will evaluate the CRT based on the time resolution (σ_{Θ}). In the first approximation the CRT equals to $2.35\sqrt{2}\sigma_{\Theta}$. However, a fundamental lower limit of the CRT is defined by the time spread due to the unknown depth of interaction (DOI) in a single scintillator. It should be stressed that this factor gains importance for large scintillator detectors, as in J-PET for example. Since the interactions may occur with nearly equal probability along the whole thickness (d) of the plastic scintillator, time spread in a single scintillator may be well approximated by the uniform distribution with the width of d/c , where c denotes the γ photon speed. This implies that the distribution of the time difference between two detected γ photons has a triangular form with FWHM equal to d/c . Therefore, the final value of the CRT may be estimated with the formula

$$\text{CRT} = \sqrt{11.04\sigma_{\Theta}^2 + \frac{d^2}{c^2}}. \quad (21)$$

As seen from equations (20)–(21), in order to evaluate σ_{Θ} , and therefore the CRT, one has to know the shape of the pdf function f_{it} to calculate the α_2 coefficient, and also the errors of the signal registered on the photomultipliers to calculate the covariance matrix S . Determination of the shape of f_{it} was discussed in the previous section. In the next section we will analyse the sources of errors in the signals $\hat{y}_{(L)}, \hat{y}_{(R)}$.

2.4. Analysis of registered signals errors

The noise contribution to the signals registered on the left ($\hat{y}_{(L)}$) and right ($\hat{y}_{(R)}$) sides of the scintillator strip is the same, and therefore in this section we will omit the L, R indices. In further analysis we assume that the noise signal v (see equation (9)) is defined as a sum of two components:

$$v = v_p + v_r, \quad (22)$$

where v_p describes the perturbations of the pdf function f_{it} , based on the limited number of input photon signals, and v_r stands for the signal recovery noise. The latter component is introduced by the procedure of signal recovery based on the limited number of registered samples of the signal in the voltage domain. The problem of signal recovery has been widely discussed in Raczyński *et al* (2015a) and (2015b). We assume that the noises v_p and v_r are uncorrelated and normally distributed with covariance matrices S_p and S_r , respectively. Thus, one may write that

$$S = S_p + S_r. \quad (23)$$

The exact values of v_p and v_r depend on the type of photomultiplier applied. In this work we consider two types of photomultiplier:

- PMT—a vacuum tube photomultiplier treated as the basic one in the current J-PET prototype,
- MCP—a microchannel plate photomultiplier.

It should be underlined that the following analysis does not include silicon photomultipliers. We have published extensive research into the possibility of application of silicon photomultipliers in the J-PET tomograph in our previous study (Moskal *et al* 2016).

Noises v_p and v_r are mainly influenced by the width of the single photoelectron contributing to the final output signal and the quantum efficiency of the photomultiplier. The most distinctive feature of the MCP photomultiplier is its ability to register the arrival time of each photon. Thus, the output signal may be evaluated by using a model of a single photon. For all types of photomultiplier we use the Gaussian model (Bednarski *et al* 2014) for the shape of signal of a single photoelectron, with width σ_p . In the experimental section we will optimize the parameter σ_p for the MCP photomultiplier, aiming to minimize the noise v_p . The quantum efficiency may be used directly to estimate the number of photoelectrons induced in the photomultiplier, N_p . In the following we will apply N_p to model the total output signal.

It is worth noting that v_r vanishes in the case of the MCP photomultiplier. There is no need to recover the output signal, since all photon arrival times are registered. In the following we will briefly describe the noises v_p and v_r .

2.4.1. *Analysis of v_p .* The registered signal y affected only by the noise v_p will be denoted by

$$\tilde{y} = y + v_p.$$

The signal \tilde{y} consists of N_p signals from individual photoelectrons:

$$\tilde{y} = \sum_{k=1}^{N_p} \tilde{y}_k. \tag{24}$$

As mentioned in section 2.4, the signal from single photoelectron \tilde{y}_k is assumed to be a Gaussian function:

$$\tilde{y}_k(n) = \frac{\beta}{\sqrt{(2\pi)N_p\sigma_p}} \exp\left(-\frac{(t^{(n)} - t_r^k)^2}{2\sigma_p^2}\right), \quad n = 1, 2, \dots, N, \tag{25}$$

where t_r^k is a random variable with distribution f_{t_r} , which denotes the registration time of the k th photon.

We aim to calculate the diagonal elements of the covariance matrix S_p :

$$S_p(n, n) = E[(\tilde{y}(n) - y(n))^2], \quad n = 1, 2, \dots, N, \tag{26}$$

where

$$\begin{aligned} E[(\tilde{y}(n) - y(n))^2] &= E[(\tilde{y}(n) - E[\tilde{y}(n)] + E[\tilde{y}(n)] - y(n))^2] \\ &= E[(\tilde{y}(n) - E[\tilde{y}(n)])^2] + (E[\tilde{y}(n)] - y(n))^2 \\ &= \text{Var}(\tilde{y}(n)) + \text{Bias}^2(\tilde{y}(n)), \quad n = 1, 2, \dots, N. \end{aligned} \tag{27}$$

According to equation (24):

$$E[\tilde{y}(n)] = N_p E[\tilde{y}_k(n)], \tag{28}$$

$$\text{Var}(\tilde{y}(n)) = N_p \text{Var}(\tilde{y}_k(n)), \quad n = 1, 2, \dots, N. \tag{29}$$

Estimates of $\text{Var}(\tilde{y}(n))$ and $\text{Bias}(\tilde{y}(n))$ were introduced in Rosenblat (1956) and Simonoff (1996). Assuming that the underlying pdf function f_{t_r} is sufficiently smooth, and that $\sigma_p \rightarrow 0$ with $N_p\sigma_p \rightarrow \infty$ as $N_p \rightarrow \infty$, the Taylor series expansion gives

$$\text{Bias}(\tilde{y}(n)) \approx \beta \frac{\sigma_p^2 f_t''(t^{(n)})}{2}, \tag{30}$$

$$\text{Var}(\tilde{y}(n)) \approx \beta^2 \frac{f_t(t^{(n)})}{2\sqrt{\pi}N_p\sigma_p}, n = 1, 2, \dots, N, \tag{31}$$

where $f_t''(t^{(n)})$ is a second derivative of the pdf function $f_t(t^{(n)})$. The above approximations may be inaccurate for finite N_p . The number of registered photoelectrons N_p is of the order of hundreds, and a detailed discussion is given in section 3.1. Therefore, a new method for evaluating $\text{Var}(\tilde{y}(n))$ and $\text{Bias}(\tilde{y}(n))$ for finite N_p should be proposed. During this study the novel concept of the estimation of requested statistics has been developed. The method is described in great detail in the appendix, where it is shown that the values of $\text{Var}(\tilde{y})$, $\text{Bias}(\tilde{y})$ may be estimated as:

$$\text{Bias}(\tilde{y}(n)) \approx \beta \left(\frac{2\Phi(t^{(n)}, \lambda\sigma_p)}{3\sqrt{2\pi}\sigma_p} - f_t(t^{(n)}) \right), \tag{32}$$

$$\text{Var}(\tilde{y}(n)) \approx \beta^2 \frac{9\Phi(t^{(n)}, \lambda\sigma_p) + 8\Phi^2(t^{(n)}, \lambda\sigma_p) - 16\Phi^3(t^{(n)}, \lambda\sigma_p)}{36\pi N_p \sigma_p^2}, n = 1, 2, \dots, N, \tag{33}$$

where λ is the parameter defining the range of the second argument of the function Φ :

$$\Phi(t^{(n)}, \lambda\sigma_p) = F_{t_r}(t^{(n)} + \lambda\sigma_p) - F_{t_r}(t^{(n)} - \lambda\sigma_p), \quad n = 1, 2, \dots, N, \tag{34}$$

and $F_{t_r}(t^{(n)})$ is the cumulative distribution function of $f_{t_r}(t^{(n)})$ calculated at $t^{(n)}$. A discussion of formulae (32) and (33) is given in the appendix.

It should be underlined that both estimation methods—the proposed ones (equations (32), (33)) and those based on Taylor series approximation (equations (30), (31))—have the same asymptotic properties. It may be shown that for $\sigma_p \rightarrow 0$ with $N_p\sigma_p \rightarrow \infty$ as $N_p \rightarrow \infty$:

$$\begin{aligned} \text{Bias}(\tilde{y}(n)) &= 0, \\ \text{Var}(\tilde{y}(n)) &= 0, \quad n = 1, 2, \dots, N. \end{aligned}$$

2.4.2. *Analysis of v_r .* We denote the signal y affected only by the v_r noise as:

$$\hat{y} = \tilde{y} + v_r. \tag{35}$$

The recovery process only takes place provided the complete output \tilde{y} is registered on a photomultiplier. If the photon arrival times are registered, as in the MCP photomultiplier, then $v_r = 0$. Recovery of the signal \hat{y} is carried out only for the PMT photomultiplier.

Details of the signal recovery process were given in Raczynski *et al* (2015a), and here only the main points will be recalled. The evaluation of the signal \hat{y} requires two steps: (i) recovery of the sparse expansion \hat{x} and (ii) calculation of \hat{y} based on \hat{x} . The relation between the solution \hat{y} and its sparse representation \hat{x} is linear:

$$\hat{y} = A\hat{x}, \tag{36}$$

where A is an orthonormal matrix. As shown in Raczynski *et al* (2015a), from the Bayes theory the properties of a regularized solution can be found, in particular its covariance matrix, denoted hereafter as $S_{r(x)}$, may be easily derived:

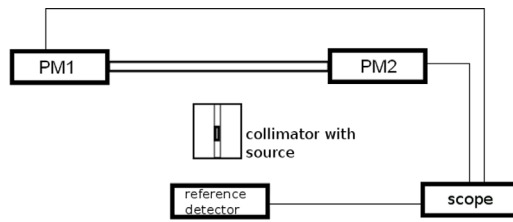


Figure 3. Scheme of the experimental setup.

$$S_{r(x)} = \left(P^{-1} + \frac{M}{\sigma^2 N} \mathbf{1} \right)^{-1} \quad (37)$$

where P is the covariance matrix of the sparse signals x , and M denotes the number of registered samples of the signals y and σ is the standard deviation of the measurement error. Finally, based on equation (36), the covariance matrix S_r is given by

$$S_r = A \left(P^{-1} + \frac{M}{\sigma^2 N} \mathbf{1} \right)^{-1} A^T. \quad (38)$$

3. Experimental results

3.1. Experimental setup

In this section we investigate the accuracy of the proposed method for evaluation of the time resolution and CRT. The model is validated by performing the experiment with a single detection module of the J-PET scanner built from the BC-420 plastic scintillator strip, with dimensions of $5 \times 19 \times 300$ mm, read out at two ends by Hamamatsu R4998 (PMT) photomultipliers. Our experimental setup is depicted in figure 3. Measurements are performed using γ photon from the ^{22}Na source placed inside the lead collimator between the scintillator strip and the reference detector. The reference detector consists of a small scintillator strip with a thickness of 4 mm. A collimated beam emerging through a slit 1.5 mm wide and 20 cm long is used for irradiating desired points across the strip. In order to detect the event, coincident registration of signals from the PM1 and a reference detector is required. Such trigger conditions enable us to select precisely the annihilation quanta that reduce the background from the deexcitation photon (1.27 MeV) to a negligible level (Moskal *et al* 2014b). The time of triggering by the reference detector is used to estimate the event arrival time. The constant electronic time delay between the true event time and the measured time of arrival at the reference detector does not influence the time resolution and is shifted to zero. The full waveforms of PMT signals are sampled using the Lecroy SDA 6000A oscilloscope running at a sampling rate of 20 Giga samples per second.

In our previous studies it was shown that the time resolution is fairly independent of the irradiation position (Moskal *et al* 2014b, 2015). Therefore, we determine the time resolution and CRT of the J-PET scanner in one position, at the center of the strip ($x = 15$ cm). In order to evaluate the experimental value of time resolution and CRT a data set of 10^4 pairs of signals from PM1 and PM2 registered in coincidence was analyzed. In the first step, for each pair of fully sampled signals from the left and right ends of the strip, $\tilde{y}_{(L)}$ and $\tilde{y}_{(R)}$, a front-end electronic device probing signals at four voltage levels, at both the rising and falling slope, was simulated. The signals $\hat{y}_{(L)}$ and $\hat{y}_{(R)}$ were recovered using eight samples of signals $\tilde{y}_{(L)}$

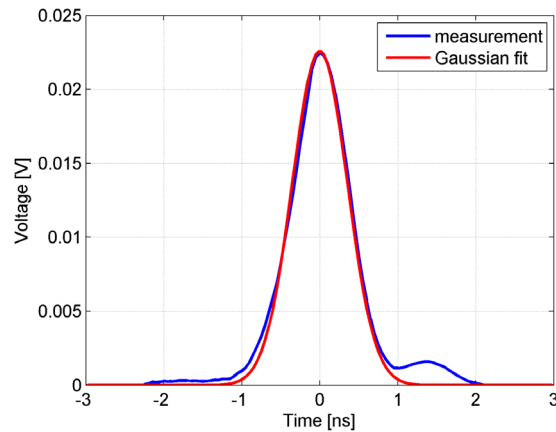


Figure 4. An example of the signal of a single photoelectron acquired with the PMT photomultiplier (blue curve) and its Gaussian fit (red curve). In the measured signal two Gaussians are observed, but the second one is much smaller and its influence on the calculated parameters is negligible.

and $\tilde{y}_{(R)}$ registered by an oscilloscope, according to the method described in section 2.4.2. For the k th pair of recovered signals $\hat{y}_{(L)}$ and $\hat{y}_{(R)}$, the energy of an event may be estimated based on the arithmetic mean of a number of photoelectrons registered at the left and right sides of the scintillator (Moskal *et al* 2014b) and is proportional to the sum of integrals of recovered signals $\hat{y}_{(L)}$ and $\hat{y}_{(R)}$. On the other hand, for the k th pair of $\hat{y}_{(L)}$ and $\hat{y}_{(R)}$, reconstruction of the time ($\hat{\Theta}_k$) and position (\hat{x}_k) was pursued by minimization of the function W in equation (12). The value of σ_{Θ} was calculated as the standard deviation of the empirical distribution of $\hat{\Theta}_k$ and was equal to about 80 ps. The corresponding value of CRT calculated based on equation (21), for a scintillator strip with a thickness of 19 mm, was equal to 275 ps. This value of CRT will be treated as the reference for the proposed approach. For clarity of presentation, we will calculate in section 3 only the CRT parameter.

According to the scheme presented in section 2.4, the evaluation of the time resolution and CRT of the PET system requires the investigation of the parameter α_2 and covariance matrix S (see equation (20)). The values of these parameters vary for different types of applied photomultipliers and are also sensitive to the position of the point of interaction of the γ photon along the scintillator strip. The values of the parameters will be provided in sections 3.1 and 3.2.

In order to model the signal at the photomultiplier output, the parameters of three pdf functions f_{i_e} , f_{i_p} and f_{i_d} , defined in equations (2), (4) and (6), respectively, must be known. It is worth noting that only the last pdf function, f_{i_d} , describes the unique properties of a given type of the photomultiplier. σ_d is delivered by the photomultiplier manufacturer: for the Hamamatsu R4998 photomultiplier (PMT) $\sigma_d = 68$ ps and for the MCP photomultiplier $\sigma_d = 40$ ps (Hamamatsu 2017). However, as our initial tests show, there is a negligible influence of the value of σ_d on the performance of the reconstruction method for the moment of γ photon interaction.

The measurement provides a discrete signal y at the photomultiplier. Repeating the time measurement under the same condition yields a set of photoelectron acquisition times (cf. equation (24)). The signal y consists of N_p Gaussian shaped signals of single photoelectrons. In figure 4 an example of a single photoelectron signal registered with the PMT photomultiplier and its Gaussian fit are shown. The signals are marked with blue and red curves,

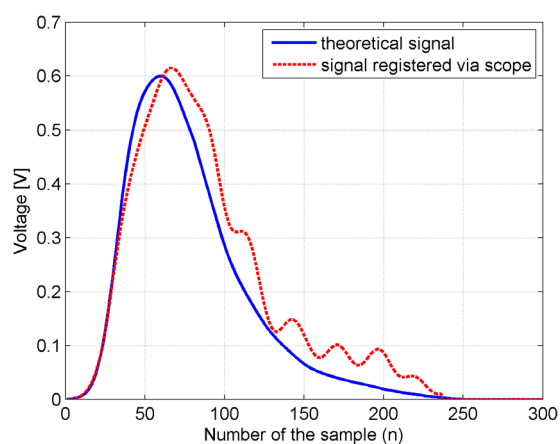


Figure 5. Signals observed in the PMT photomultiplier output generated by interaction in the center of the scintillator strip; the theoretical signal y (see equation (8)) is marked with the blue curve, and an example of signal \tilde{y} registered by the oscilloscope (see equation (24)) is marked with a red dashed curve (the meaning of variable n is the same as in formula (7)).

respectively. The standard deviation σ_p of this function is reported in Bednarski *et al* (2014) to be equal to 300 ps for a PMT photomultiplier. However, different numbers of photoelectrons (N_p) are registered due to the different quantum efficiencies. In the following we will briefly recall the main results of our earlier works, enabling us to estimate properly the number N_p . The light yield of plastic scintillators amounts to about 10 000 photons per 1 MeV of deposited energy. The 511 keV γ photon may deposit a maximum of 341 keV via Compton scattering (Szymanski *et al* 2014), which corresponds to the emission of about 3410 photons. On the other hand, in order to decrease the noise due to scattering of a γ photon inside patient's body, a minimum energy deposition of about 200 keV is required (Moskal *et al* 2012). Therefore, the range of the number of emitted photons discussed hereafter in this article is 2000–3410. Experiments conducted with PMT photomultipliers have revealed that about 280 photoelectrons are produced from the emission of 3410 photons (Moskal 2014). According to the pre-selected range (2000 to 3410 photons), the average number of emitted photons is about 2700. This number corresponds to $N_p = 220$ registered photoelectrons with the PMT photomultiplier. Since the CRT of the J-PET system will be determined at the center of the strip, the numbers of photoelectrons N_p contributing to the signals induced on the left and right scintillator ends are the same, and are equal to 110.

As mentioned at the beginning of section 2, the values of τ_d , τ_r and σ_e of the pdf function f_e were adjusted based on experimental studies with a single BC-420 scintillator strip. We have carried out numerous tests for various strips of the BC-420 scintillator type and found that the values of the estimated parameters of the f_e pdf function were consistent within the measurement errors. Therefore, the signals evaluated based on the proposed model, presented in section 2.2, have shapes very similar to those registered by an oscilloscope during the experiment (see figure 5). In figure 5, the theoretical signal y at the center of the strip, evaluated from equation (8), is presented. The parameter β (see formula (8)) was selected in such way that the amplitude of the signal is equal to the mean amplitude of signals registered at the center of the strip ($x = 15$ cm). The analytical solution for the function f_t is difficult to find due to internal convolution in the function f_e (see equation (2)). Therefore, numerical

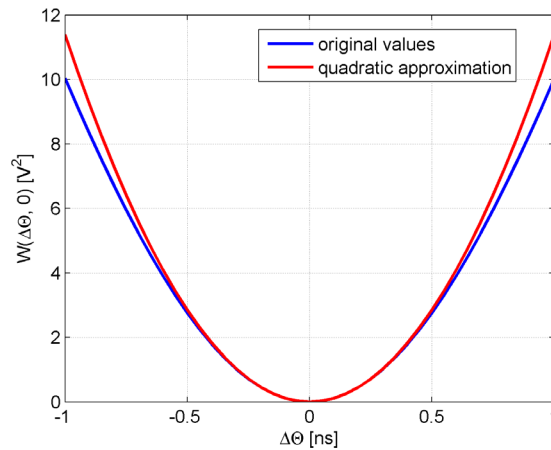


Figure 6. The shape of $W(\Delta\Theta, 0)$ near to the minimum.

evaluation of a convolution operation was applied. The signals y and \tilde{y} in figure 5 are shown in the discrete domain for discrete time samples and the curves connecting points are plotted to guide the eye.

Information about the signal y may be directly applied to evaluate the value of the parameter α_2 . In this work we are interested only in determination of the CRT of the J-PET system, and we assume that the position of the γ photon interaction is known exactly (see equation (18)). Therefore, for a fixed position of interaction, the signal y may be shifted only in the time domain due to the error of time measurement $\Delta\Theta$. For $\Delta\Theta = 0$ the theoretical and registered signals overlap and $W(\Delta\Theta, 0) = 0$ (see equation (12)). In order to evaluate α_2 , the error $\Delta\Theta$ was varied from -1 to 1 ns. For each value of $\Delta\Theta$, the function $W(\Delta\Theta, 0)$ was evaluated based on the shape of signal y shown in figure 5. The resulting, experimental function $W(\Delta\Theta, 0)$ is presented in figure 6 by a blue curve (see also equation (12)).

According to equation (18), the experimental function $W(\Delta\Theta, 0)$ may be approximated near $\Delta\Theta = 0$ by a quadratic function. The quadratic approximation of the $W(\Delta\Theta, 0)$ function is marked in figure 6 by a red curve and the coefficient of the second-order polynomial function is equal to $11.2 \frac{\text{V}^2}{\text{ns}^2}$.

3.2. Verification of method for estimating signal \tilde{y}

According to the assumptions in section 2.4, two main contributors to the signal noise are v_p and v_r . v_r was estimated in Raczynski et al (2015a) and will be recalled at the end of this section. Here, a detailed study of the method for approximating $\text{Var}(\tilde{y}(n))$ and $\text{Bias}(\tilde{y}(n))$ will be carried out. The proposed method (see equations (32) and (33)) will be compared with the well-known approximation technique based on Taylor series expansion (see equations (30) and (31)). The Monte Carlo (MC) simulation will be provided as a reference for the results of both analytical approaches.

The MC simulation was carried out for a constant number of photoelectrons, $N_p = 220$, registered by the PMT photomultiplier. In order to simulate $\text{Var}(\tilde{y}(n))$ and $\text{Bias}(\tilde{y}(n))$, only one timestamp of the original signal y , corresponding to the maximum value of 0.6V (see figure 5), was used. The analysis of the maximum value in signal y allows one to evaluate the main contribution to the covariance matrix S_p ; as seen from figure 9, the location of the maximum

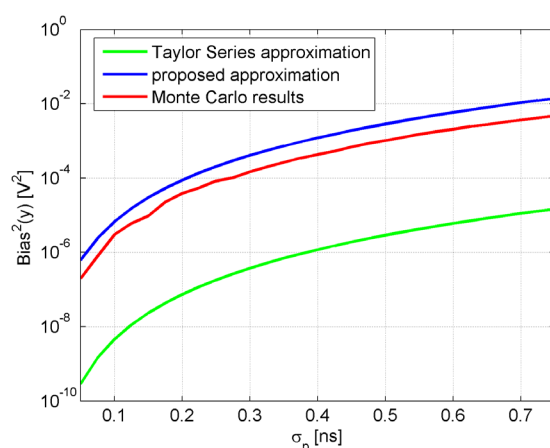


Figure 7. Comparison of the estimation of $\text{Bias}^2[\tilde{y}]$ with two analytical approaches: the proposed one (blue curve) and one based on Taylor series expansion (green curve). The reference characteristics were obtained with the Monte Carlo simulation (red curve).

value of the signal y corresponds to the location of the maximum value on the diagonal of the covariance matrix S_p . The maximum value of the original signal y is observed in the sample $n = 60$ (see figure 5). In the first step of MC simulation the random values of photon registration times t_r^k ($k = 1, 2, \dots, N_p$) were selected according to the f_r distribution. Next, the values of all N_p functions $\tilde{y}_k(60)$ were evaluated based on equation (25) and summed up, giving $\tilde{y}(60)$. The above-mentioned procedure was repeated 10^6 times for different values of σ_p from 50 ps to 750 ps with a step of 25 ps. The range of $\sigma_{|imp}$ was selected after preliminary calculations taking into account the expected number of registered photoelectrons in the J-PET scenario. Based on the large number of samples of $\tilde{y}(60)$, accurate estimation of bias and variance was possible. The resulting $\text{Bias}^2(\tilde{y}(60))$ and $\text{Var}(\tilde{y}(60))$ are shown in figures 7 and 8, respectively.

The reference values of $\text{Bias}^2(\tilde{y}(60))$ and $\text{Var}(\tilde{y}(60))$ obtained with MC simulation are marked by red curves in figures 7 and 8, respectively. The approximations of $\text{Var}(\tilde{y})$ for the proposed method and the method based on Taylor series expansion (blue and green curves, respectively) are very similar to the reference curve for small values and tend to differ for larger values of σ_p . However, in the most interesting region, for σ_p equal to about 300 ps, the proposed method is more accurate than the one based on the Taylor series, and the values of $\text{Var}(\tilde{y})$ are equal to $6.5 \times 10^{-3} V^2$ and $7.0 \times 10^{-3} V^2$, respectively (the reference value of $\text{Var}(\tilde{y})$ from MC simulation is equal to $5.1 \times 10^{-3} V^2$). Comparison of the $\text{Bias}^2(\tilde{y})$ and $\text{Var}(\tilde{y})$ curves reveals the fundamental relation between variance and bias. The variance dominates for smaller values of σ_p and becomes comparable with bias for σ_p at a level of about 500 ps (compare the red curves in figures 7 and 8). For σ_p larger than 500 ps, the total error is mostly influenced by the bias. It is worth noting that the method based on the Taylor series significantly underestimates the values of $\text{Bias}^2(\tilde{y})$ (see figure 7), which leads to an underestimation of the overall error.

3.3. Evaluation of the time resolution of the J-PET system

In the first step we compare the covariance matrices S_p and S_r (see equations (22) and (23)) according to the description in section 3.1 and using our previous study (Raczyński *et al* 2015a). The resulting values of the diagonal elements of S_p and S_r are shown in figure 9.

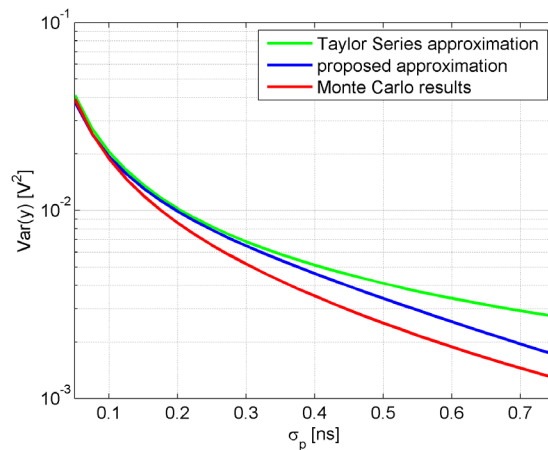


Figure 8. Comparison of the estimation of $\text{Var}[\bar{y}]$ with two analytical approaches: the proposed one (blue curve) and one based on Taylor series expansion (green curve). The reference characteristics were obtained with the Monte Carlo simulation (red curve).

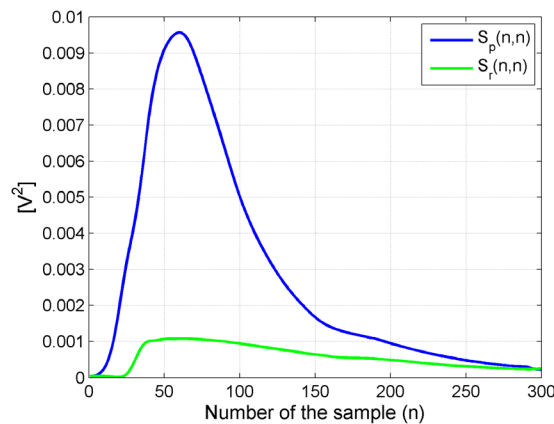


Figure 9. Comparison of the diagonal elements of the covariance matrices S_p and S_r for the PMT photomultiplier.

Theoretical values of S_p were evaluated as in section 3.2 for PMT and the results are marked in figure 9 by a blue curve. The values of elements of S_r are marked by a green curve in figure 9. The comparison of the resulting characteristics with the shape of the pdf function f_{t_r} , presented in figure 5, indicates that the reconstructed errors S_p and S_r are strongly related to the signal value. The maximum values of the diagonal elements of S_p and S_r occur near to the maximum of signal y (figure 5). On the other hand, analysis of the characteristics plotted in figure 9 reveals that the error introduced by the limited number of photoelectrons in the registered signal (S_p) is a dominating factor.

In order to compare the reconstructed values of the covariance matrices S_{rmp} and S_r , we use the trace (Tr) of the covariance matrix since diagonality is assumed. The values of $\text{Tr}(S_p)$ and $\text{Tr}(S_r)$ for different photomultiplier types are gathered in table 1. In the following we will analyse the value of $\text{Tr}(S_p)$ as the function of the number of registered photoelectrons (N_p) and the standard deviation of the single photoelectron signal (σ_p). The resulting characteristics

Table 1. Summary of theoretical CRT calculations for the J-PET scanner. The parameters are described in the text. The presented values of CRT take into account an additional smearing of the time due to the unknown depth of interaction in a scintillator strip with a thickness of 19 mm (see equation (21) for details).

Parameter	Unit	Photomultiplier type			
		PMT		MCP	
N_p	1	220	220	350	700
σ_p	ps	300	500	420	360
$\sigma_{p(\text{opt})}$	ps	500	500	420	360
$\text{Tr}(S_p)$	V^2	0.73	0.55	0.39	0.23
$\text{Tr}(S_r)$	V^2	0.22	0.0	0.0	0.0
$\text{Tr}(S)$	V^2	0.95	0.55	0.39	0.23
CRT	ps	290	260	215	170

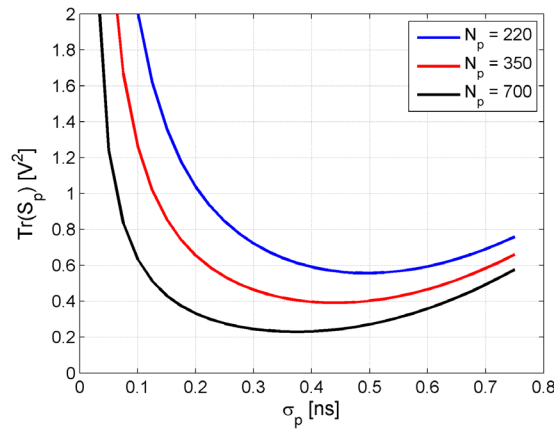


Figure 10. Trace of the S_p matrix as a function of the standard deviation of a single photoelectron signal (σ_p) for three specified numbers of registered photoelectrons $N_p = 220, 350$ and 700 .

of $\text{Tr}(S_p)$ as a function of σ_p are shown in figure 10. The values of $\text{Tr}(S_p)$ were calculated for three specified numbers of registered photoelectrons (220, 350 and 700) and are marked in figure 10 by blue, red and black curves, respectively. The smallest value of N_p is specific for the PMT photomultiplier, as mentioned in section 3.1. The highest number, $N_p = 700$, indicates the maximum number of registered photoelectrons in the experimental scenario, and was selected in order to demonstrate the best theoretical resolution of J-PET. Results in figure 10 show that all the $\text{Tr}(S_p)$ functions, evaluated for a given number of registered photoelectrons, have a minimum. The shape of the $\text{Tr}(S_p)$ functions illustrates the fundamental trade-off between variance and bias, as mentioned in section 3.2. Hence, for given number of registered photoelectrons it is possible to adjust the optimal value of σ_p , denoted hereafter by $\sigma_{p(\text{opt})}$. Comparison of the $\sigma_{p(\text{opt})}$ values for three N_p values in figure 10 shows that the larger the number of registered photoelectrons the smaller the value of $\sigma_{p(\text{opt})}$. For instance, for the PMT photomultiplier that registers 220 photoelectrons on average, the minimum error occurs for $\sigma_{p(\text{opt})} = 500$ ps (blue curve in figure 10). For the PMT photomultiplier σ_p is not a variable, and has fixed value of about 300 ps. However, the MCP photomultiplier registers timestamps of the signal instead of the complete signal. Therefore, the value of $\sigma_{p(\text{opt})}$ of each contributing

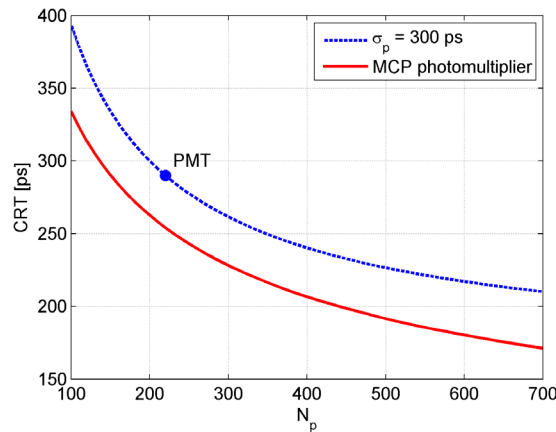


Figure 11. Theoretical calculations of CRT versus the number of photoelectrons N_p , of the J-PET tomograph equipped with two types of photomultipliers: PMT and MCP. The presented values of CRT take into account an additional smearing of the time due to the unknown depth of interaction in a scintillator strip with a thickness of 19 mm (see equation (21) for details).

signal may be adjusted according to the number of registered timestamps (N_p). In that sense, optimization of $\sigma_{p(\text{opt})}$ for the MCP photomultiplier may be obtained. Simulations using the f_r function give a $N_p^{-4.1}$ dependence of $\sigma_{p(\text{opt})}$ on the number of photoelectrons.

In general, the MCP photomultiplier is capable of registering all the timestamps of the photons that reach the scintillator end. In order to account for possible inefficiency of the MCP, we determine the characteristics of J-PET equipped with a MCP in the range $100 \leq N_p \leq 700$. First, for a given number N_p , the optimal value of $\sigma_{p(\text{opt})}$ was estimated based on the characteristics of $\text{Tr}(S_p)$ (see figure 10). Next, the matrix S_p was calculated based on the proposed technique (see equations (32) and (33)). Finally, σ_Θ was evaluated based on equation (20). In the case of MCP, $\text{Tr}(S_r) = 0$, since the output signal is given directly based on the measured timestamps and the assumed shape of the single photoelectron signal. The resulting CRT characteristics are shown by the red solid line in figure 11. The presented CRT values take into account an additional smearing of the time due to the unknown depth of interaction in a scintillator strip with a thickness of 19 mm (see equation (21) for details).

Additionally, the CRT calculated for $\sigma_p = 300$ ps (the shape of single photoelectron signal characteristic for the PMT photomultiplier), also including the v_r error introduced by the signal recovery procedure $\text{Tr}(S_r) = 0.22 V^2$ reported in Raczyński *et al* (2015a), is marked by a blue dashed line in figure 11. The theoretical value of CRT for the PMT photomultiplier is marked with a full circle on the blue curve, for $N_p = 220$. The theoretical CRT of the J-PET scanner with a PMT photomultiplier is about 290 ps and agrees with the experimental CRT value, reported to be about 275 ps (Raczyński *et al* 2015a). For a fixed value of the quantum efficiency (equivalent to the number N_p), further improvement of CRT is possible by the application of MCP photomultipliers. In the wide range of numbers of registered photoelectrons shown in figure 11, improvement of about 30 ps is observed (red and blue dashed curves). The presented results show that the best theoretical CRT of the J-PET scanner with 30 cm long strips is estimated for the MCP photomultiplier capable of registering all timestamps of arrival for 700 photons, is at the level of 170 ps. The main results of the study as well as the parameters of the analysed photomultipliers, are summarized in table 1.

4. Extension of the proposed method to conventional PET systems

The proposed framework for calculation of the time resolution and CRT may also be applied to state of the art PET scanners equipped with crystal scintillators. For this purpose, in order to estimate the time resolution, function W , introduced in equation (12), has to be adapted to the new situation. First of all, during reconstruction of the time of γ photon interaction ($\hat{\Theta}$), only signals from one side of the crystals are acquired (in the J-PET scanner two signals are registered at both ends of scintillator). Moreover, due to the small size of the crystals, only reconstruction of the interaction time $\hat{\Theta}$ is carried out; the function W is one-dimensional. Therefore, the function W is defined as

$$W(\Delta\Theta) = (y - \hat{y})(y - \hat{y})^T.$$

Finally the standard deviation σ_{Θ} is given by the formula

$$\sigma_{\Theta} = \sqrt[4]{\frac{\sum_{n=1}^N S^2(n, n)}{\alpha_2^2}}, \quad (39)$$

which differs from equation (20) only by a factor $\sqrt[4]{2}$. In order to evaluate time resolution and CRT, one has to evaluate the distribution time of photon registration at the photomultiplier (t_r) to calculate the α_2 coefficient, and also the errors of the signal registered on the photomultipliers to calculate the covariance matrix S .

In the case of PET scanners with inorganic crystal scintillators, the description of the photon registration time t_r at the photomultiplier includes two random components t_e and t_d :

$$t_r = t_e + t_d.$$

Compared with J-PET, here the propagation time of the photon along the scintillator (t_p) may be neglected due to the small size of the single crystal. Therefore, the only difference in calculation of t_r is the evaluation of the distribution of t_e . The main parameter that governs the speed of light emission after the absorption of a γ photon is the decay time. Crystal materials show decay pulse shapes that are single- or multi-exponential. For example, for BGO crystals a bi-exponential shape is observed for the distribution of time t_e (Seifert *et al* 2012).

On the other hand, determination of the time resolution, defined in equation (39), requires information about the covariance matrix S of the registered signal \hat{y} . In section 2.4 we derived an analytical description for the main components of the covariance matrix S , i.e. the matrices S_p and S_r .

The formula for calculation of elements of the S_p matrix, describing the perturbations of the distribution function f_r based on a limited number of registered photoelectrons, given in equation (26), may also be applied to the PET scanners with crystal scintillators. The only differences are in the parameters describing the shape of the f_r distribution function and the expected number of photoelectrons (N_p) while including the light yield of crystal scintillators.

The latter component, matrix S_r , is introduced by the procedure of signal recovery based on the limited number of registered samples of the signal in the voltage domain. The J-PET system involves a four-threshold sampling method to generate samples of a signal waveform. An example of a similar electronic system for probing the signals in a voltage domain, coupled with an experimental setup equipped with LSO crystals, was developed in Kim *et al* (2009). The waveforms of signals were read out by the oscilloscope, and an electronic system for probing these signals in a voltage domain with four thresholds was applied to reconstruct the pulse shape. This scheme allows evaluation of all the parameters required to calculate the

signal recovery error, according to the formula given in equation (38), for the PET system with crystal scintillators.

5. Conclusions

In this paper we have introduced a new method for estimating the time resolution and CRT of the J-PET system using only simulations which were tested based on data from a single detector module. This is particularly useful for the design of expensive devices. For the J-PET tomograph the most expensive part of the system is the photomultipliers. In this work two types of photomultiplier were simulated: vacuum tube photomultipliers and microchannel plates.

The basic idea of the method is the use of the statistical nature of the whole signal acquisition process. We have highlighted three statistical phenomena: the emission of photons in the scintillator strip, the propagation of light pulses along the strip and registration of light in photomultipliers. Parameters of the probability density functions were selected in order to properly describe light pulses from the BC-420 plastic scintillator.

An important aspect of our work concerns the statistical analysis of a reconstruction error of the probability density function based on the set of single photoelectron signals. In this work dependences of the overall variance and bias on the number and width of the single photoelectron signals were evaluated. The proposed estimation method was validated using the Monte Carlo simulation and it was shown that the obtained results are consistent. Moreover, the proposed technique was demonstrated to be more accurate than the literature approach (Rosenblat 1956, Simonoff 1996). The developed estimation scheme is general and may be incorporated elsewhere.

In the experimental section, the method of time resolution and CRT estimation was tested using signals registered by means of the single detection module of the J-PET scanner. In order to evaluate the CRT of the J-PET detector we incorporated the method described in Raczynski *et al* (2015a). In the cited work, the CRT obtained with the experimental scheme with vacuum tube photomultipliers was reported to be equal to about 275 ps. Our calculation shows that application of the proposed estimation method can give very similar result of about 290 ps. The consistency of the experimental and theoretical results obtained for the J-PET scanner equipped with vacuum tube photomultipliers suggests that the estimated CRTs for other photomultipliers are reliable. The CRTs determined for the detector with microchannel plates were 215 ps and 170 ps, assuming photomultiplier quantum efficiencies of 50% and 100%, respectively.

Future work will investigate other aspects of the signal acquisition process by using the proposed statistical model, for example the influence of the distribution parameters of the photon emission time on time resolution. In this study, the distribution parameters were selected in order to describe the properties of light signals observed in the BC-420 plastic scintillator. However, our group have developed a novel type of plastic scintillator and examined the influence of the chemical composition of the plastic scintillator on the overall performance of the J-PET detector (Wieczorek *et al* 2015a, 2015b, Wieczorek *et al* 2016). Application of the proposed model to that task enables us to directly use information about the shape of the distribution of the time of photon emission to predict the CRT of the J-PET detector.

Acknowledgments

We acknowledge technical and administrative support of A Heczko, M Kajetanowicz, W Migdał and financial support from the Polish National Center for Development and Research through grant INNOTECH-K1/IN1/64/159174/NCBR/12, the Foundation for Polish Science through the MPD program, the EU and MSHE grant no. POIG.02.03.00-161

00-013/09, Doctus—the Lesser Poland PhD Scholarship Fund, and the Marian Smoluchowski Kraków Research Consortium ‘Matter-Energy-Future’. B Hiesmayr acknowledges gratefully the Austrian Science Fund FWF-P26783.

Appendix. Kernel density estimation

The function \tilde{y}_k , describing the k th signal from a single photoelectron, given in equation (25), may be approximated by

$$\tilde{y}_k(n) \approx \begin{cases} \frac{\beta}{\sqrt{(2\pi)N_p\sigma_p}} \left(1 - \frac{(t^{(n)} - t_r^k)^2}{\lambda^2\sigma_p^2}\right) & t_r^k \in (t^{(n)} - \lambda\sigma_p, t^{(n)} + \lambda\sigma_p) \\ 0 & \text{otherwise} \end{cases} \quad (\text{A.1})$$

where $n = 1, 2, \dots, N$ and λ contributes to the signal width. The probability that the random variable $\tilde{y}_k(n)$ is equal to the specified value may be calculated based on the previously introduced function Φ (see equation (34)). In particular, the probability that the random variable $\tilde{y}_k(n) = 0$ is equal to $1 - \Phi(t^{(n)}, \lambda\sigma_p)$; the k th registration time t_r^k is out of range $(t^{(n)} - \lambda\sigma_p, t^{(n)} + \lambda\sigma_p)$ (see the second case in equation (A.1)). Denoting the first case in equation (A.1) with u_k :

$$u_k(n) = \frac{\beta}{\sqrt{(2\pi)N_p\sigma_p}} \left(1 - \frac{(t^{(n)} - t_r^k)^2}{\lambda^2\sigma_p^2}\right), \quad n = 1, 2, \dots, N, \quad (\text{A.2})$$

we may write that for $n = 1, 2, \dots, N$ the expected value of $\tilde{y}_k(n)$ is equal to

$$\begin{aligned} E[\tilde{y}_k(n)] &= E[u_k(n)]\Phi(t^{(n)}, \lambda\sigma_p) + E[0](1 - \Phi(t^{(n)}, \lambda\sigma_p)) \\ &= E[u_k(n)]\Phi(t^{(n)}, \lambda\sigma_p), \end{aligned} \quad (\text{A.3})$$

and the variance of $\tilde{y}_k(n)$ is equal to

$$\begin{aligned} \text{Var}(\tilde{y}_k(n)) &= E[(u_k(n) - E[u_k(n)])^2]\Phi(t^{(n)}, \lambda\sigma_p) + E[(0 - E[u_k(n)])^2](1 - \Phi(t^{(n)}, \lambda\sigma_p)) \\ &= \text{Var}(\tilde{u}_k(n))\Phi(t^{(n)}, \lambda\sigma_p) + E[u_k(n)]^2(1 - \Phi(t^{(n)}, \lambda\sigma_p)). \end{aligned} \quad (\text{A.4})$$

In order to simplify the further calculations the following assumption is proposed. Note that in most interesting cases the range $(t^{(n)} - \lambda\sigma_p, t^{(n)} + \lambda\sigma_p)$, is narrow compared with the estimated pdf function f_{t_r} domain. Therefore, the pdf function f_{t_r} is considered to be uniform in the range $(t^{(n)} - \lambda\sigma_p, t^{(n)} + \lambda\sigma_p)$:

$$f_{t_r}(\epsilon) \simeq \text{const.} \quad \epsilon \in (t^{(n)} - \lambda\sigma_p, t^{(n)} + \lambda\sigma_p). \quad (\text{A.5})$$

It is worth noting that the smaller the ratio of the single-signal to overall signal width the better the performance of the proposed approximation method.

Under the assumption in equation (A.5), the required moments in equations (A.3) and (A.4), $E[u_k(n)]$, $E[u_k(n)]^2$ and $\text{Var}(\tilde{u}_k(n))$, can be easily derived. After some simple calculations the equations for the expected value and the variance of the random variable $\tilde{y}_k(n)$ are given by

$$\begin{aligned} E(\tilde{y}(n)) &\approx \beta \frac{2\Phi(t^{(n)}, \lambda\sigma_p)}{3\sqrt{2\pi}\sigma_p}, & n = 1, 2, \dots, N, \\ \text{Var}(\tilde{y}(n)) &\approx \beta^2 \frac{9\Phi(t^{(n)}, \lambda\sigma_p) + 8\Phi^2(t^{(n)}, \lambda\sigma_p) - 16\Phi^3(t^{(n)}, \lambda\sigma_p)}{36\pi N_p\sigma_p^2}, & n = 1, 2, \dots, N. \end{aligned}$$

References

- Bednarski T *et al* 2014 Calibration of photomultipliers gain used in the J-PET detector *Bio-Algorithms Med-Syst.* **10** 13
- Candes E, Romberg J, Tao T 2006 Robust uncertainty principles: Exact signal reconstruction from highly incomplete frequency information *IEEE Trans. Inf. Theory* **52** 489
- Conti M 2009 State of the art and challenges of time-of-flight PET *Phys. Med.* **25** 1
- Conti M 2011 Focus on time-of-flight PET: the benefits of improved time resolution *Eur. J. Nucl. Med. Mol. Imaging* **38** 1147
- DeGroot M 1986 *Probability and Statistics* (Reading, MA: Addison-Wesley) p 420
- Donoho D 2006 Compressed sensing *IEEE Trans. Inf. Theory* **52** 1289
- Eljen Technology 2017 www.eljentechnology.com
- Hamamatsu 2017 www.hamamatsu.com
- Humm J L, Rosenfeld A and Del Guerra A 2003 From PET detectors to PET scanners *Eur. J. Nucl. Med. Mol. Imaging* **30** 1574
- Karp J *et al* 2008 Benefit of time-of-flight in PET: experimental and clinical results *J. Nucl. Med.* **49** 462
- Kim H *et al* 2009 A multi-threshold sampling method for TOF-PET signal processing *Nucl. Instrum. Methods A* **602** 618
- Moskal P *et al* 2011 Novel detector systems for the positron emission tomography *Bio-Algorithms Med-Syst.* **7** 73
- Moskal P *et al* 2012 TOF-PET detector concept based on organic scintillators *Nucl. Med. Rev.* **15** C81
- Moskal P *et al* 2014a A novel TOF-PET detector based on organic scintillators *Radiother. Oncol. Proc. Suppl.* **110** S69
- Moskal P *et al* 2014b Test of a single module of the J-PET scanner based on plastic scintillators *Nucl. Instrum. Methods A* **764** 317
- Moskal P *et al* 2015 A novel method for the line-of-response and time-of-flight reconstruction in TOF-PET detectors based on a library of synchronized model signals *Nucl. Instrum. Methods A* **775** 54
- Moskal P *et al* 2016 Time resolution of the plastic scintillator strips with matrix photomultiplier readout for J-PET tomograph *Phys. Med. Biol.* **61** 2025
- Moszynski M and Bengtson B 1977 Light pulse shapes from plastic scintillators *Nucl. Instrum. Methods A* **142** 417
- Moszynski M and Bengtson B 1979 Status of timing with plastic scintillation detectors *Nucl. Instrum. Methods A* **158** 1
- Palka M *et al* 2014 A novel method based solely on FPGA units enabling measurement of time and charge of analog signals in positron emission tomography *Bio-Algorithms Med-Syst.* **10** 41
- Parzen E 1962 On estimation of a probability density function and mode *Ann. Math. Stat.* **33** 1065
- Raczynski L *et al* 2014 Novel method for hit-position reconstruction using voltage signals in plastic scintillators and its application to positron emission tomography *Nucl. Instrum. Methods A* **764** 186
- Raczynski L *et al* 2015a Compressive sensing of signals generated in plastic scintillators in a novel J-PET instrument *Nucl. Instrum. Methods A* **786** 105
- Raczynski L 2015b Reconstruction of signal in plastic scintillator of PET using Tikhonov regularization *Proc. IEEE Engineering in Medicine and Biology Conf.* p 2784
- Rosenblatt M 1956 Remarks on some nonparametric estimates of a density function *Ann. Math. Stat.* **27** 832
- Saint Gobain Crystals 2017 www.crystals.saint-gobain.com
- Seifert S, van Dam H and Schaart D 2012 The lower bound on the timing resolution of scintillation detectors *Phys. Med. Biol.* **57** 1797
- Simonoff J 1996 *Smoothing Methods in Statistics* (New York: Springer)
- Słomka P, Pan T, Germano G 2016 Recent advances and future progress in PET instrumentation *Semin. Nucl. Med.* **46** 5
- Spanoudaki V and Levin C 2011 Investigating the temporal resolution limits of scintillation detection from pixellated elements: comparison between experiment and simulations *Phys. Med. Biol.* **56** 735
- Szymanski K *et al* 2014 Simulations of gamma quanta scattering in a single module of the J-PET detector *Bio-Algorithms Med-Syst.* **10** 71
- Tikhonov A 1963 Solution of incorrectly formulated problems and the regularization method *Sov. Math.—Dokl.* **4** 1035
- Tikhonov A and Arsenin V 1977 *Solutions of Ill-Posed Problems* (Washington, DC: Winston and Sons)

- Townsend D 2004 Physical principles and technology of clinical PET imaging *Ann. Acad. Med. Singap.* **33** 133
- Wieczorek A *et al* 2015a PALS investigations of free volumes thermal expansion of J-PET plastic scintillator synthesized in polystyrene matrix *Nukleonika* **60** 777
- Wieczorek A *et al* 2015b A pilot study of the novel J-PET plastic scintillator with 2-(4-styrylphenyl) benzoxazole as a wavelength shifter *Acta Phys. Pol. A* **127** 1487
- Wieczorek A *et al* 2016 Novel plastic scintillators for the fully digital and MRI compatible J-PET scanner *Phys. Med.: Eur. J. Med. Phys.* **32** 232